

JOURNAL OF ADVANCED APPLIED SCIENCES

e-ISSN: 2979-9759



RESEARCH ARTICLE

Photodetection Performance of Hydrothermally Grown *n*-ZnO Nanorods at High Illumination Intensity

Sedat Kurnaz^{1™} • Bilge Merve Candan² • Ozgur Ozturk² •

ARTICLE INFO

Article History

Received: 19.06.2023 Accepted: 29.06.2023 First Published: 30.06.2023

Keywords

Hydrothermal Photodetector Photoresponse Solar light ZnO Nanorod



An ultraviolet photodetector based on hydrothermally grown ZnO nanorods (NRs) on a ZnO thin film sandwich structure is reported here. A thin film of ZnO is deposited on a p-Si(100) substrate by means of RF sputter. ZnO NRs are prepared by the hydrothermal method on n-ZnO/p-Si at a molarity (10 mM) and growth times (2 and 3 h) at 90 °C. The surface texture is also investigated by scanning electron microscopy. The diameters of the ZnO-NRs are found to be in the range of 36 nm to 63 nm. Current versus time (I(t)) measurements are performed under the high illumination intensities (50 and 100 mW/cm²) and the bias voltages (1, 5, and 10 V). The parameters responsivity (R), sensitivity (S), decay time (τ_d), and rise time (τ_r), are calculated. Despite the slow τ_d and τ_r , the samples prepared at 2 h in 10 mM solution perform best due to their high S and R. In particular, the S for the Z2 varies between 0.12 and 1.93, while for the Z3 it varies between 0.10 and 0.94. The R is 1.36 AW⁻¹ for the Z2, and 0.69 AW⁻¹ for the Z3.



Please cite this paper as follows:

Kurnaz, S., Candan, B. M., & Ozturk, O. (2023). Photodetection performance of hydrothermally grown *n*-ZnO nanorods at high illumination intensity. *Journal of Advanced Applied Sciences*, 2(1), 30-35. https://doi.org/10.29329/jaasci.2023.562.04

1. Introduction

Ultraviolet photodetectors (UV PDs) have become an important research topic in recent years due to their wide range of civil and military applications such as imaging systems, flame detection, atmospheric ozone detection, space communications and early missile warning systems (Hirano et al., 2001; Sandvik et al., 2001; Pau et al., 2006; Torres et al., 2007; John & Blum, 2011; Jeong et al., 2013; Chen et al., 2015; Chen et al., 2018; Liang et al., 2020). UV PDs based on wide bandgap materials such as GaN (Jiang et al., 2015), SiC (Chen

et al., 2007) and ZnO (Echresh et al., 2015) have a visible-blind advantage over silicon photodiodes. Among these materials, a large number of studies in the literature have focused on ZnO as a promising semiconducting material for a possible UV PD (Li et al., 2013; Ali et al., 2014). In particular, ZnO can be grown as various types of one-dimensional (1D) nanostructures such as nanocombs, nanorods (NRs), nanobelts, nanoflowers and nanopillars. Among them, ZnO NRs have received the most attention due to their electron confinement properties, high surface-to-volume ratio, good crystallinity and the polar nature of the 1D nanostructure (Alsultany et al., 2016; Ozturk et al.,

E-mail address: sedatkurnaz@kastamonu.edu.tr

¹Kastamonu University, Central Research Laboratory, Kastamonu/Türkiye

²Kastamonu University, Faculty of Engineering and Architecture, Department of Electrical and Electronics Engineering, Kastamonu/Türkiye

[™] Corresponding author

2022). Despite their remarkable advantages, ZnO NRs based on PDs have a long decay time in the second scale due to the oxygen-related hole trap states at the nanorod surface (Soci et al., 2007; Hu et al., 2012). The performance of PDs can be improved by varying the morphological structure of ZnO NRs. For example, Lin et al. (2016) prepared hydrothermally grown ZnO NRs PD on Si (100) substrate using a range of precursor concentrations. The sensitivity and responsivity are observed to increase with an increase in the precursor concentration increased. Lee et al. (2016) developed ZnO NR-based PD on SiO₂ passivation layer. The experimental results show that the PD exhibits a slow rise/decay time (55.5/33.1 s), a responsivity (0.102 AW⁻¹) at a bias of 5V. The passivation layer is also applied to improve the light response of the PDs. Compared to non-passivated devices, the passivated device exhibits faster rise and decay times.

In this context, we have investigated the photodetector properties of ZnO NR-based PDs. The hydrothermal method is used to fabricate ZnO NRs on n-ZnO/p-Si with a molarity (10 mM) and growth times (2 and 3 h). The photodetector properties such as decay time (τ_d), rise time (τ_r), responsivity (R) and sensitivity (S) parameters are investigated by applying solar light illumination intensities (50 and 100 mW/cm²) and bias voltages (1, 5 and 10 V).

2. Materials and Methods

ZnO seed layers with a thickness of 100 nm were deposited on p-Si(100) substrates with a resistivity of 1-10 Ω .cm using RF sputter (NVTS 400, Nanovak). Prior to RF sputtering, the substrates were immersed in a solution of HF+20.H₂O for 30 s to remove native oxides and quenched in deionized (DI) water. The substrates were then ultrasonically clean using ethanol and DI water. The RF sputter was performed at a temperature of 50 °C with a ZnO target. The pressure of the Ar:O₂ (80:20) gas was set at 10 mTorr. The RF power output was fixed at 100 W. The base vacuum pressure of the sputtering system was set at 1×10^{-6} Torr. Immediately after deposition, the samples were immediately annealed at 600 °C for 30 min in an air ambient air.

A hydrothermal method was used to grow ZnO NRs on the ZnO seed layer. The n-ZnO/p-Si substrates were placed in 30 ml of a growth solution of DI water with zinc acetate dihydrate (Zn(CH₃COO)₂.2H₂O) and hexamethylenetetramine (C₆H₁₂N₄)

in an equimolar molar concentration (10 mM). The autoclave was kept in an oven at a temperature of 90 °C for a period of 2 h and 3 h. At the end of the reaction, the samples were washed with DI water to remove any residual salts and organic matter. They were then dried in an oven at 90 °C.

100 nm of aluminum (Al) metal was deposited as a Schottky or rectifier contact by DC sputter (NVTS 400, Nanovak) on the top of a ZnO NRs/ZnO seed layer. These were circular dots with a diameter of 2 mm. The deposition chamber was evacuated to a pressure of 40 mTorr under Ar gas and the DC power was fixed at 135 W. The samples were classified according to growth times (2 and 3 h). They were referred to as Z2 and Z3 PDs.

The dimension and orientation of the NRs were evaluated by scanning electron microscopy (SEM; FEI Quanta FEG 250). The current-time (I(t)) measurements as a function of solar light intensity (50 and 100 mW/cm²) and bias voltage (1, 5, and 10 V) were performed using a Keithley 2400 source meter and a solar simulator (Scientech SF300A). The wavelength of the 300 W Xenon lamp of the solar simulator was in the range of 300 nm to 2000 nm, which was used to measure the photocurrent. The solar light with a frequency of 1.62 Hz was dropped by a mechanical chopper. A schematic illustration of the fabricated Al/ZnO NRs/n-ZnO/p-Si based PD under the illumination of solar light is shown in Figure 1(a).

3. Results and Discussion

Top view SEM images of the Z2 and Z3 PDs are shown in Figure 1(b) and (c). ZnO NRs grown on ZnO layer/p-Si are seen. The average diameters of the NRs of the Z2 and Z3 samples are 63 nm and 36 nm, respectively. Although prepared at the same molarity and temperature in terms of production parameters, the diameter of the NRs is reduced by half when the growth time is increased from 2 h to 3 h. At the same time, these SEM images show that the NRs grow both vertically and tilted. The main reason for this situation is that the grains of ZnO used as the seed layer is not all in the (002) direction, which is the growth orientation of the nanorods. This causes the NRs to grow in a tilted form. Furthermore, the quality of ZnO NRs is affected by several factors such as precursor concentration, growth time, seed layer thickness, pH of the growth solution, and growth temperature (Khan & Kim, 2017; Abdulrahman, 2020).



Figure 1. (a) Schematic illustration of the *n*-ZnO/*p*-Si PD, SEM images of (b) Z2, and (c) Z3 PDs.

Important parameters used to evaluate the performance of the fabricated PDs are R, S, τ_r and τ_d . The photocurrent (I_{ph}) suddenly increases and reaches saturation as the solar light drops onto the PD at an average frequency of 1.62 Hz. The photocurrent is expressed as:

$$I_{ph} = Aq(\Delta n_{ph} \nu_n - \Delta p_{ph} \nu_p)$$
(1)

Where; Δn_{ph} and Δp_{ph} are the mean electron and hole densities generated by the solar radiation, and v_n and v_p are the mean electron and hole velocities. As the electric field strength in the depletion region increases with an increase in the bias voltage, the average velocity of the electrons and holes will be higher. This leads to higher photocurrents at higher bias voltages (Luo et al., 2006). The current returns to its initial value when the solar light is switched off. It has been observed that the amount of photocurrent generated increases as the intensity of the illumination is increased.

S, defined in Eq. (2) (Farooqi & Srivastava, 2019), is the ratio of the photocurrent (I_{ph}) to the dark current. R is defined in Eq. (3) (Abdulrahman, 2020) as the ratio of the photocurrent (I_{ph}) to the optical power (P_{opt}) incident on the active area of the PDs device.

$$S = \frac{I_{ph} - I_{drk}}{I_{drk}} \tag{2}$$

$$R = \frac{I_{ph}}{P_{opt}A} \tag{3}$$

 τ_r is defined as time taken to increase photocurrent from 10% to 90% of its maximum increase value in Eq. (4), while τ_d is time taken to reach 10% of 90% maximum increase in Eq. (5) (Khokhra et al., 2017; Farooqi & Srivastava, 2019).

$$\tau_r = \tau_{\%90} - \tau_{\%10} \tag{4}$$

$$\tau_d = \tau_{\%10} - \tau_{\%90} \tag{5}$$

Figure 2 shows the I(t) measurements of the Z2 at a light intensity of 50 mW/cm² and 100 mW/cm² and a bias of 1, 5 and 10 V. When a 1 V bias is applied, the dark current is 0.85 μ A. At 50 mW/cm² and 100 mW/cm², it increases to 93 μ A and 96 μ A, respectively. At 5 V bias, the dark current is 0.6 mA. The currents are 0.99 mA and 1.01 mA as the light intensity increases. At a bias of 10 V, the dark current is 1.40 mA, but at a light intensities of 50 mW/cm² and 100 mW/cm² it has values of 3.50 mA and 3.90 mA, respectively (Table 1).

The I(t) curves obtained at 1, 5, and 10 V bias under 50 mW/cm² and 100 mW/cm² for the Z3 are shown in Figure 2. At 1 V bias, the dark current is 63 μ A. At 50 mW/cm² and 100 mW/cm², it increases to 70 μ A and 71 μ A, respectively. The dark current is 0.57 mA at 5 V bias. At 50 mW/cm² and 100 mW/cm², it is 0.76 mA and 0.80 mA, respectively. While it is 1.20 mA in the dark at 10 V bias, it is 10.0 mA and 12.0 mA when illuminated at 50 mW/cm² and 100 mW/cm².

The values of R, S, τ_r , and τ_d , parameters of the fabricated PDs calculated from the I(t) measurements in Figure 2 are listed in Table 2. When 1 V bias is applied to the Z2 under 50 mW/cm² and 100 mW/cm², the τ_r is 63.3 ms. When 10 V bias is applied, it is 73.6 ms and 62 ms. The τ_d is 96 ms and 117 ms with a bias of 1 V at the light intensities of 50 mW/cm² and 100 mW/cm² respectively, while they are 77 ms and 78 ms with a bias of 10 V. The τ_d decreases with increasing bias at both light levels. The S increases with increasing light intensity and bias from 0.12 to 1.84 at a light intensity of 50 mW/cm² and from 0.13 to 1.93 at a light intensity of 100 mW/cm². The R increases to 1.36 AW¹¹ and 0.82 AW¹¹ with increasing light intensity and bias. The R increases with increasing light intensity and bias to 1.36 AW¹¹ and 0.82 AW¹¹.



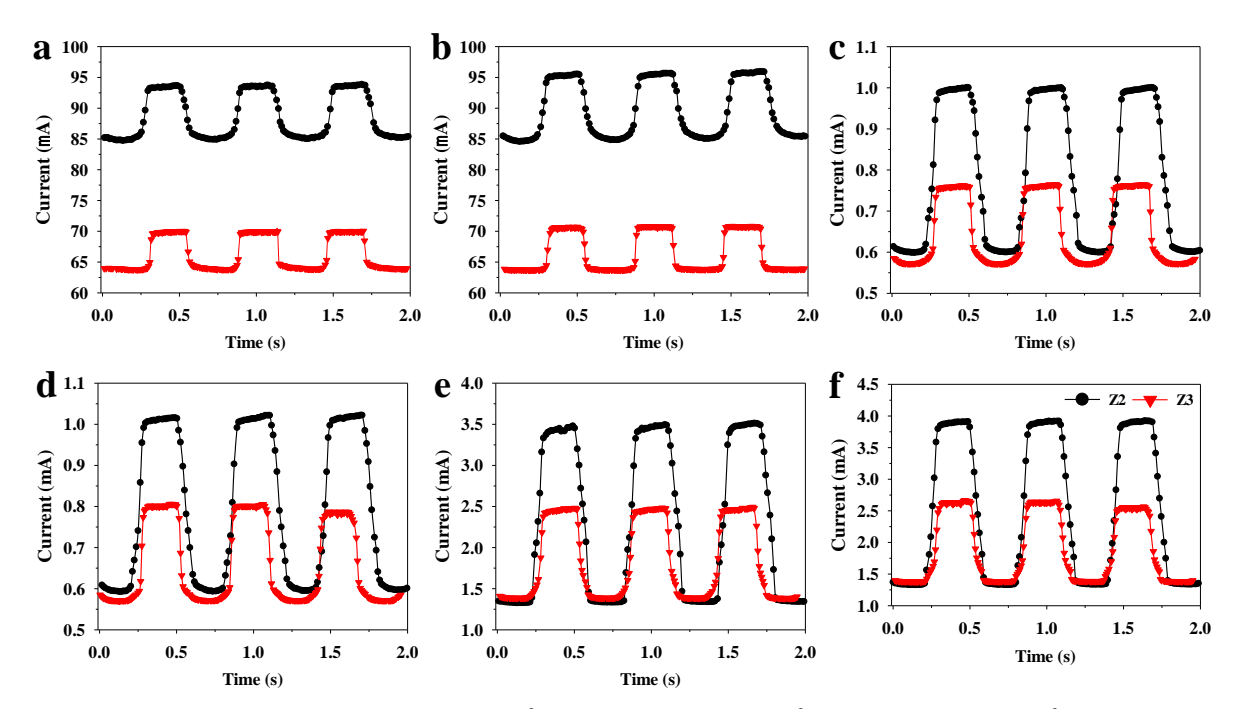


Figure 2. The *I*(*t*) measurements of (a) 1 V at 50 mW/cm², (b) 1 V at 100 mW/cm², (c) 5 V at 50 mW/cm², (d) 5 V at 100 mW/cm², (e) 10 V at 50 mW/cm², and (f) 10 V at 100 mW/cm².

Table 1. Current values depending on light intensity and bias voltage.

~ ~	D1 (T1)	D 1 (1)	G	G () () () () () () ()
Name	Bias (V)	Dark current (mA)	Current (mA) at 50 mW/cm ²	Current (mA) at 100 mW/cm ²
	1	0.085	0.093	0.096
Z 2	5	0.60	0.99	1.01
	10	1.40	3.50	3.90
	1	0.063	0.070	0.071
Z3	5	0.57	0.76	0.80
	10	1.20	10.0	12.0

At light intensities of 50 mW/cm² and 100 mW/cm², when a bias voltage of 1 V is applied to the Z3, the τ_r is 32 ms and 26 ms respectively, while it increases from 60 ms to 69 ms at a bias of 10 V. As the bias increases, the τ_r increases. The τ_d is 59 ms

and 22 ms at 1 V bias, and 65 ms and 69.6 ms at 10 V bias for 50 mW/cm² and 100 mW/cm² light intensities, respectively. The τ_r increases with increasing bias. The *R* increases to 0.69 AW-1 and 0.41 AW-1 with increasing light intensity and bias.

Table 2. Photoresponse properties of ZnO NR-based PDs.

Name	Power density (mW/cm ²)	Bias (V)	Rise time (ms)	Decay time (ms)	Sensitivity	Responsivity (AW-1)
Z2		1	63.3 ± 6.0	96.0±7.0	0.12	0.006
	50	5	70.6±0.3	83.0±3.5	0.76	0.25
		10	73.6±1.8	77.0 ± 6.2	1.84	1.36
		1	63.3±5.7	117.0±7.8	0.13	0.003
	100	5	73.0±1.5	91.0±6.7	0.72	0.13
		10	62.0±1.1	78.0 ± 6.2	1.93	0.82
Z3		1	32.0±4.2	59.0±5.8	0.10	0.004
	50	5	43.0±3.0	63.6 ± 3.0	0.33	0.12
		10	60.0 ± 0.3	65.0 ± 2.9	0.78	0.69
		1	26.0±3.7	22.0±1.6	0.11	0.002
	100	5	35.0 ± 7.6	61.0 ± 10.6	0.39	0.07
		10	69.0±2.0	69.6±5.7	0.94	0.41



4. Conclusion

A hydrothermal process is used to successfully grow ZnO NRs on n-ZnO/p-Si. The diameters of the ZnO NRs are found to be in the range of 36-63 nm from the SEM images. Under solar illumination intensities (50 and 100 mW/mm²) and bias voltages (1, 5 and 10 V), the photoresponse characteristics of the ZnO NRs based PDs are investigated. It is observed that the parameters R, S, τ_r , and τ_d are influenced by the fabricated PDs at 90 °C with a molarity (10 mM) and growth times (2 and 3 h). The Z2 and Z3 reach the saturation level of the photocurrent at all the bias voltages below 50 mW/cm² and 100 mW/cm², respectively. In comparison, the τ_r and τ_d of the Z2 are 62-73.6 ms and 77-117 ms respectively. The τ_r and τ_d of the Z3 are 26-69 and 22-69.6 ms, respectively. The S for the Z2 is between 0.12 and 1.93, while for the Z3 it is between 0.10 and 0.94. The R is 1.36 AW⁻¹ for Z2 and 0.69 AW⁻¹ for Z3. The sample prepared at 2 h in 10 mM solution performs best due to its high S and R, despite its slow τ_d and τ_r .

Acknowledgment

This research was supported by Kastamonu University Scientific Research Projects Coordination Department under the Grant No. KU-BAP01/2019-36 and KU-BAP01/2018-106.

Conflict of Interest

The authors declare that they have no conflict of interest.

References

- Abdulrahman, A. F. (2020). The effect of different substrateinclined angles on the characteristic properties of ZnO nanorods for UV photodetectors applications. *Journal of Materials Science: Materials in Electronics*, *31*, 14357– 14374. https://doi.org/10.1007/s10854-020-03995-3
- Ali, G. M., Moore, J. C., Kadhim, A. K., & Thompson, C. (2014). Electrical and optical effects of Pd microplates embedded in ZnO thin film based MSM UV photodetectors: A comparative study. Sensors and Actuators A: Physical, 209, 16–23. https://doi.org/10.1016/j.sna.2014.01.010
- Alsultany, F. H., Hassan, Z., & Ahmed, N. M. (2016). A high-sensitivity, fast-response, rapid-recovery UV photodetector fabricated based on catalyst-free growth of ZnO nanowire networks on glass substrate. *Optical Materials*, 60, 30–37. https://doi.org/10.1016/j.optmat.2016.07.004
- Chen, X., Zhu, H., Cai, J., & Wu, Z. (2007). High-performance 4H-SiC-based ultraviolet p-i-n photodetector. *Journal of Applied Physics*, 102(2), 024505. https://doi.org/10.1063/1.2747213
- Chen, H., Liu, K., Hu, L., Al-Ghamdi, A. A., & Fang, X. (2015). New concept ultraviolet photodetectors.

- *Materials Today*, 18(9), 493–502. https://doi.org/10.1016/j.mattod.2015.06.001
- Chen, M., Zhao, B., Hu, G., Fang, X., Wang, H., Wang, L., Luo, J., Han, X., Wang, X., Pan, C., & Wang, Z. L. (2018). Piezo-phototronic effect modulated deep UV photodetector based on ZnO-Ga₂O₃ heterojuction microwire. *Advanced Functional Materials*, 28(14), 1706379. https://doi.org/10.1002/adfm.201706379
- Echresh, A., Chey, C. O., Zargar Shoushtari, M., Khranovskyy, V., Nur, O., & Willander, M. (2015). UV photo-detector based on p-NiO thin film/n-ZnO nanorods heterojunction prepared by a simple process. *Journal of Alloys and Compounds*, 632, 165–171. https://doi.org/10.1016/j.jallcom.2015.01.155
- Farooqi, M. M. H., & Srivastava, R. K. (2019). Effect of annealing temperature on structural, photoluminescence and photoconductivity properties of ZnO thin film deposited on glass substrate by sol–gel spin coating method. *Proceedings of the National Academy of Sciences, India Section A: Physical Sciences*, 90, 845–859. https://doi.org/10.1007/s40010-019-00648-x
- Hirano, A., Pernot, C., Iwaya, M., Detchprohm, T., Amano, H., & Akasaki, I. (2001). Demonstration of flame detection in room light background by solar-blind AlGaN PIN photodiode. *Physica Status Solidi (a)*, *188*(1), 293–296. https://doi.org/10.1002/1521-396x(200111)188:1<293::aid-pssa293>3.0.co;2-d
- Hu, L., Yan, J., Liao, M., Xiang, H., Gong, X., Zhang, L., & Fang, X. (2012). An optimized ultraviolet-a light photodetector with wide-range photoresponse based on ZnS/ZnO biaxial nanobelt. *Advanced Materials*, 24(17), 2305–2309. https://doi.org/10.1002/adma.201200512
- Jeong, S., Nam, J. W., Ahn, K. B., Park, I. H., Kim, S. W., Lee, J., & Yashin, I. (2013). Slewing mirror telescope optics for the early observation of UV/optical photons from gamma-ray bursts. *Optics Express*, 21(2), 2263. https://doi.org/10.1364/oe.21.002263
- Jiang, Z., Zhang, W., Luo, A., Atalla, M. R. M., You, G., Li, X., Wang, L., Liu, J., Elahi, A. M., Wei, L., Zhang, Y., & Xu, J. (2015). Bias-enhanced visible-rejection of GaN Schottky barrier ultraviolet photodetectors. *IEEE Photonics Technology Letters*, 27(9), 994–997. https://doi.org/10.1109/lpt.2015.2399302
- John, H., & Blum, M.-M. (2011). Review of UV spectroscopic, chromatographic, and electrophoretic methods for the cholinesterase reactivating antidote pralidoxime (2-PAM). *Drug Testing and Analysis*, 4(3-4), 179–193. https://doi.org/10.1002/dta.327
- Khan, W., & Kim, S.-D. (2017). Ultra-violet photo-response characteristics of p -Si/i -SiO₂/ n-ZnO heterojunctions based on hydrothermal ZnO nanorods. *Materials Science in Semiconductor Processing*, 66, 232–240. https://doi.org/10.1016/j.mssp.2017.04.031



- Khokhra, R., Bharti, B., Lee, H.-N., & Kumar, R. (2017). Visible and UV photo-detection in ZnO nanostructured thin films via simple tuning of solution method. *Scientific Reports*, 7(1), 15032. https://doi.org/10.1038/s41598-017-15125-x
- Lee, S. H., Kim, S. H., & Yu, J. S. (2016). Metal-semiconductor-metal near-ultraviolet (~380 nm) photodetectors by selective area growth of ZnO nanorods and SiO2 passivation. *Nanoscale Research Letters*, 11(1). https://doi.org/10.1186/s11671-016-1541-3
- Li, Q., Wei, L., Xie, Y., Zhang, K., Liu, L., Zhu, D., Jiao, J., Chen, Y., Yan, S., Liu, G., & Mei, L. (2013). ZnO nanoneedle/H₂O solid-liquid heterojunction-based self-powered ultraviolet detector. *Nanoscale Research Letters*, 8(1), 415. https://doi.org/10.1186/1556-276x-8-415
- Liang, W., Shi, Z., Li, Y., Ma, J., Yin, S., Chen, X., Wu, D., Tian, Y., Zhang, Y., Li, C. X., & Shan, C. (2020). Strategy of all-inorganic Cs₃Cu₂I₅/Si-Core/Shell nanowires heterojunction for stable and ultravioletenhanced broadband photodetectors with imaging capability. *ACS Applied Materials & Interfaces*, 12, 37363–37374. https://doi.org/10.1021/acsami.0c10323
- Lin, C. M., Cheng, N. J., Hung, S. C., & Li, Y. M. (2016). Effect of solution on one-step hydrothermal growth of ZnO nanorod arrays and its application to ultraviolet photodetectors. *Journal of Nano Research*, 40, 46–57. https://doi.org/10.4028/www.scientific.net/jnanor.40.4

- Luo, L., Zhang, Y., Mao, S. S., & Lin, L. (2006). Fabrication and characterization of ZnO nanowires based UV photodiodes. *Sensors and Actuators A: Physical*, *127*(2), 201–206. https://doi.org/10.1016/j.sna.2005.06.023
- Ozturk, O., Candan, B. M., Kurnaz, S., Cicek, O., & Tasci, A. T. (2022). Solar light performances of n-ZnO nanorods/p-Si-based photodetectors under high illumination intensity. *Journal of Material Science: Materials in Electronics*, 33, 15222–15231. https://doi.org/10.1007/s10854-022-08440-1
- Pau, J. L., Anduaga, J., Rivera, C., Navarro, Á., Álava, I., Redondo, M., & Muñoz, E. (2006). Optical sensors based on III-nitride photodetectors for flame sensing and combustion monitoring. *Applied Optics*, *45*(28), 7498. https://doi.org/10.1364/ao.45.007498
- Sandvik, P., Mi, K., Shahedipour, F., McClintock, R., Yasan, A., Kung, P., & Razeghi, M. (2001). Al_xGa_{1-x}N for solar-blind UV detectors. *Journal of Crystal Growth*, 231(3), 366–370. https://doi.org/10.1016/s0022-0248(01)01467-1
- Soci, C., Zhang, A., Xiang, B., Dayeh, S. A., Aplin, D. P. R., Park, J., Bao, X. Y., Lo, Y. H. & Wang, D. (2007). ZnO nanowire UV photodetectors with high internal gain. *Nano Letters*, 7(4), 1003–1009. https://doi.org/10.1021/nl070111x
- Torres, O., Tanskanen, A., Veihelmann, B., Ahn, C., Braak, R., Bhartia, P. K., Veefkind, P., & Levelt, P. (2007). Aerosols and surface UV products from ozone monitoring instrument observations: An overview. *Journal of Geophysical Research*, 112(D24). https://doi.org/10.1029/2007jd008809

